REPORT DOCUMENTATION PAGE

Form Approved
OMB No. 0704-0188

1. REPORT DATE *(DD-MM-YYYY)*	2. REPORT TYPE	3. DATES COVERED *(From - To)*
8/31/2008	Final Report	6/1/07-5/31/08

4. TITLE AND SUBTITLE
Exploratory study of MM-wave patch antennas for strain measurement and crack detection

5a. CONTRACT NUMBER
FA9550-07-1-0465

5b. GRANT NUMBER

5c. PROGRAM ELEMENT NUMBER

6. AUTHOR(S)
Haiying Huang

JC Chiao

Ronald Carter

5d. PROJECT NUMBER

5e. TASK NUMBER

5f. WORK UNIT NUMBER

7. PERFORMING ORGANIZATION NAME(S) AND ADDRESS(ES)

University of Texas at Arlington
500 W. First Street, WH211
Arlington, TX 76019

8. PERFORMING ORGANIZATION REPORT NUMBER

9. SPONSORING / MONITORING AGENCY NAME(S) AND ADDRESS(ES)
Air Force Office of Scientific Research
875 N. Randolph St., Room 3112
Arlington, VA 22203-1954

10. SPONSOR/MONITOR'S ACRONYM(S)
AFOSR

11. SPONSOR/MONITOR'S REPORT NUMBER(S)
AFRL-OSR-VA-TR-2012-0441

12. DISTRIBUTION / AVAILABILITY STATEMENT

A

13. SUPPLEMENTARY NOTES

14. ABSTRACT

The feasibility of applying patch antennas for strain measurement was investigated. The relationship between the antenna resonant frequency and strains applied along the electrical length and width direction of a patch antenna was derived analytically, based on transmission line mode. A dual-frequency patch antenna was designed and fabricated using conventional photolithography techniques. The application of the patch antenna for strain measurement was evaluated by bonding the patch antenna to an aluminum cantilever beam and applying loads at the free end of the cantilever beam. The shifts of the return loss S_{11} curves under loads were correlated to the strains experienced by the patch antenna. The strain sensitivity of the antenna obtained from experimental measurements agreed well with the analytical prediction. Research issues associated with interrogating the antenna resonant frequency using a monostatic radar system is also discussed.

15. SUBJECT TERMS

16. SECURITY CLASSIFICATION OF:			17. LIMITATION OF ABSTRACT	18. NUMBER OF PAGES	19a. NAME OF RESPONSIBLE PERSON
a. REPORT	b. ABSTRACT	c. THIS PAGE		14	Haiying Huang
					19b. TELEPHONE NUMBER *(include area code)* 817-272-0563

Exploratory study of MM-wave patch antennas for strain measurement and crack detection-Final Report

PI: Haiying Huang, Dept. of Mechanical and Aerospace Engineering, University of Texas at Arlington
Co-PIs: Ronald L Carter and JC Chiao, Dept. of Electrical Engineering, University of Texas at Arlington
Participating students: Uday Tata and Shanchali Deb

Abstract: The goal of this project is to prove the strain sensing capability of a patch antenna. With integrated sensing and data transmitting capabilities, the patch antennas have great potentials to serve as passive wireless strain sensor. The linear relationship between the antenna resonant frequency and the applied strain was derived analytically. The procedures for designing the patch antenna and fabricating them using conventional photolithography techniques were established. The application of the patch antenna for strain measurement was evaluated by bonding the patch antenna to an aluminum cantilever beam and applying loads at the free end of the cantilever beam. The strain sensitivity of the antenna was estimated to be 15 kHz/microstrain. The experimental measurements matched very well with the analytical prediction. Noncontact interrogation of the antenna resonant frequency using a monostatic radar system was also investigated. Research issues related to this noncontact interrogation technique is discussed. Two graduate students, Uday Tata and Shanchali Deb, worked in this project, under the supervision of the PIs. The project resulted in a journal submission, a provisional patent submission, a Master thesis, and a conference paper.

1. Introduction

Structural Health Monitoring (SHM) is a technology critical for the safety assurance of mechanical, aerospace, and civil structures. By performing autonomous inspection of structures using embedded sensors, a SHM system can provide advanced warnings that prevent catastrophic structural failures. Strain is one of the most important mechanical parameters acquired by SHM systems. By monitoring strain changes in load-bearing structures, the factors that could potential cause structural failures such as excessive loading, vibration, crack development, and environmental aging, *etc.* can be detected.

Various strain sensors have been developed in the past. A detailed review of different strain sensing mechanisms can be found in the literature. The most commonly used strain sensor is the piezoresistive thin film strain gauge. However, since SHM systems usually require a network of strain sensors in order to obtain a distributed assessment of the structural condition, thin film strain gauges are not favorable for SHM systems because of the complexity and weight penalty associated with the wiring of these strain gauges. Optical fiber-based strain sensors, on the other hand, are an attractive choice of sensor for SHM systems due to their compact size, light weight, remote accessibility, multiplexing capability, and immunity to electromagnetic interferences. Even though many optical fiber strain sensors have been implemented for various SHM applications, the inherent shortcomings of optical fiber sensors, *e.g.* expensive interrogation equipment, limited strain range, and fragility, *etc.*, have not been resolved.

Recently, wireless strain sensors are becoming more and more popular for SHM systems. These sensors, equipped with embedded microprocessors and wireless communication capabilities, have the potential to reduce the installation and maintenance costs of distributed sensor networks. Many of these wireless sensors require batteries to be operational. Therefore, their life spans are limited by the battery life. Passive wireless sensors are attractive alternatives because they do not

require any power supply. These passive wireless sensors usually consist of a sensing unit and a data transmitting unit. The electromagnetic (EM) impedance of the sensing unit varies with the physical measurand. When it is connected to an antenna, the EM impedance change of the sensing unit shifts the resonant frequency of antenna. This frequency shift is then remotely interrogated using inductive coupling. Because the sensing unit is not integrated with the antenna, these passive wireless sensors are usually quite large in size.

In this project, we demonstrated that a patch antenna itself can serve as the sensing unit for strain measurement. With integrated sensing and data transmitting capability, the size of the antenna sensor can be reduced significantly. The relationship between the applied strain and the resonant frequency of the patch antenna is first derived. The design, fabrication, and evaluation of a dual frequency patch antenna for strain measurement are then discussed. The agreement between the simulated and measured strain sensitivities proved the feasibility of applying patch antennas for strain sensing.

2. Principle of operation

The patch antenna, as shown in Figure 1, consists of a layer of dielectric substrate, a rectangular patch printed on one side of the substrate, and a ground plane coated on the other side of the substrate. The rectangular patch and the ground plane, both made of conductive metals, form an EM resonant cavity that radiates at a specific resonant frequency. Based on the transmission line model, the resonant frequency of a rectangular patch antenna is calculated as

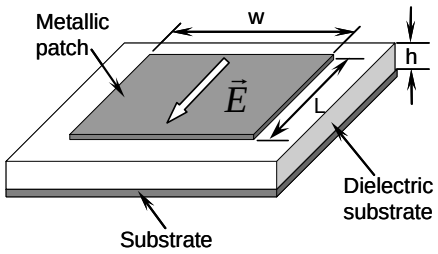

Figure 1: Patch antenna.

$$f_{res} = \frac{c}{2\sqrt{\varepsilon_{re}}} \frac{1}{L_e + 2\Delta L_{oc}}, \qquad (1)$$

where c is the velocity of light. The electrical length Le of the antenna is defined as the dimension of the metallic patch along the direction of the radiation mode. The effective dielectric constant ε_{re} is related to the dielectric constant of the substrate ε_r, the substrate thickness h, and the electrical width of the patch w_e, *i.e.*

$$\varepsilon_{re} = \frac{\varepsilon_r + 1}{2} + \frac{\varepsilon_r - 1}{2\sqrt{(1 + 10h / w_e)}}. \qquad (2)$$

The line extension ΔL_{oc} is calculated from the effective dielectric constant ε_{re}, the substrate thickness h, and the electric width w_e,

$$\Delta L_{oc} = 0.412h \frac{(\varepsilon_{re} + 0.3)(w_e / h + 0.264)}{(\varepsilon_{re} - 0.258)(w_e / h + 0.813)}. \qquad (3)$$

Assuming the antenna is subjected to a tensile strain ε_L along its electrical length direction, the patch width and the substrate thickness will change due to Poisson's effect, *i.e.*

$$w_e = (1 - \upsilon_p \varepsilon_L) w_{e0}, \text{ and } h = (1 - \upsilon_s \varepsilon_L) h_0. \qquad (4)$$

If the Poisson's ratios of the metallic patch and the substrate material, υ_p and υ_s, are the same, the ratio w_e/h remains to be a constant as the tensile strain ε_L changes. As a result, ε_{re} in equation (2) is independent of ε_L and ΔL_{oc} in equation (3) is proportional to the substrate thickness h. Therefore, the resonant frequency in equation (1) can be expressed as

$$f_{res} = \frac{c}{2\sqrt{\varepsilon_{re}}} \frac{1}{L_e + 2\Delta L_{oc}} = \frac{C_1}{L_e + C_2 h}, \tag{5}$$

where $C_1 = \frac{c}{2\sqrt{\varepsilon_{re}}}$ and $C_2 = 0.812 \frac{(\varepsilon_{re} + 0.3)(w_e / h + 0.264)}{(\varepsilon_{re} - 0.258)(w_e / h + 0.813)}$. The strain-induced elongation, therefore, will shift the antenna resonant frequency. At an unloaded state, the antenna frequency f_{res0} is calculated from the antenna length L_{e0} and substrate thickness h_0, i.e.,

$$f_{resO} = \frac{C_1}{L_{e0} + C_2 h_O}. \tag{6}$$

Under a strain ε_L, the antenna frequency shifts to

$$f_{res}(\varepsilon_L) = \frac{C_1}{L_{eO}(1 + \varepsilon_L) + C_2 h_O (1 - \upsilon \varepsilon_L)} \tag{7}$$

Combining equations (6) and (7), we can establish the relationship between the strain ε_L and the frequency shift Δf_{res}, *i.e.*

$$\varepsilon_L = -\frac{L_O + \upsilon_s C_2 h_O}{L_O + C_2 h_O} \frac{\Delta f_r}{f_r} = C \frac{\Delta f_{res}}{f_{res}}, \tag{8}$$

where $\Delta f_{res} = f_{res} - f_{res0}$. Analyzing the constant C indicates that the strain sensitivity of antenna is strongly governed by the dielectric constant of the substrate material.

For a positive strain ε_L, the antenna resonant frequency will shift to a lower frequency because of the elongation of its electrical length. A strain applied along the antenna's electrical width direction, however, will increase the antenna resonant frequency due to the Possion's effect. Therefore, f_{res} is more sensitive to strains applied along the electrical length direction than those applied along the electrical width direction. If the antenna is fed with an electric field polarized parallel to its geometric length direction, the electrical length L_e is the same as the geometric length L of the antenna. Rotating the electric field polarization by 90°, however, will switch the electrical length to the antenna's geometric width w. By feeding the antenna with two orthogonal electric fields, an antenna that is sensitive to strains along both directions of the antenna patch can be achieved.

3. Antenna design

In order to feed the patch antenna with two orthogonal electric fields, a dual-frequency patch antenna was designed. For a dual frequency antenna, the radiation mode with its polarized electric fields parallel to the geometric length direction of the metallic patch is denoted as the TM_{10} mode while the radiation mode whose electric fields are along the geometric width direction of the metallic patch is designated as the TM_{01} mode. For a chosen substrate thickness h and a relative dielectric constant ε_r, the dimensions of the antenna patch are calculated from the resonant frequencies corresponding to these two radiation modes. Denoting the resonant frequency for the TM_{10} mode as f_{10}, the geometric length of the antenna patch can be calculated from equation (1) as

$$L = \frac{c}{2 f_{10} \sqrt{\varepsilon_{re}}} - 2\Delta L_{oc}. \tag{9}$$

Similarly, the geometric width of the antenna patch is calculated from the resonant frequency f_{01} of the TM_{01} mode, *i.e.*

$$w = \frac{c}{2 f_{01} \sqrt{\varepsilon_{re}}} - 2\Delta w_{oc}, \tag{10}$$

where the line extension Δw_{oc} is calculated from equation (3) by replacing w with L. For a 50 μm thick polyimide substrate with a relative permittivity of 3.4, a dual frequency patch antenna operating at f_{10} = 15 GHz and f_{01} = 20 GHz will result in a metallic patch with a length of 5.33 mm and a width of 4 mm.

The patch antenna can be fed using either a contact or a non-contact technique. Since this paper is focused on proving the feasibility of the patch antenna for strain sensing, the contact technique was adopted. In order to excite the two orthogonal radiation modes simultaneously, the patch antenna has to be fed at a proper position. For the coordinated system given in Figure 2.a, only the TM_{10} mode will be excited if the patch antenna is fed at any point along $y = w/2$. The optimum position of the feeding point x_0 is determined by impedance matching, *i.e.*,

$$x_0 = \frac{L}{\pi} \cos^{-1}\left(\sqrt{\frac{50}{R_{iny}}}\right), \tag{11}$$

where the calculation of antenna impedance R_{iny} is given by Balanis (2005). Similarly, only the TM_{01} mode can be excited if the antenna is fed at a point along $x = L/2$. The feeding position y_0 for TM_{01} excitation is again calculated from the antenna impedance R_{inx}, *i.e.*

$$y_0 = \frac{w}{\pi} \cos^{-1}\left(\sqrt{\frac{50}{R_{inx}}}\right). \tag{12}$$

Feeding the patch antenna at (x_0, y_0) excites both radiation modes and matches the impedances of the patch antenna at the two resonant frequencies, f_{10} and f_{01} (Chen and Wong 1996). In order to facilitate mechanical testing of the patch antenna, the patch antenna was designed to be fed using a microstrip line, as shown in Figure 2.b. The microstrip line joins the metallic patch at (*0*, y_0), which means only the impedance of the patch antenna for the TM_{01} mode is matched. The length and the width of the microstrip line were tuned to achieve the optimum return losses at the two resonant frequencies. The final design of the dual frequency patch antenna is shown in Figure 2.b.

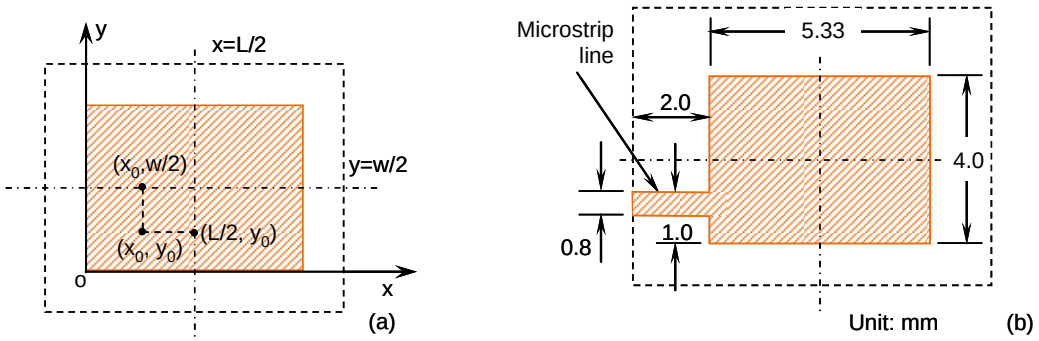

Figure 2: Antenna feeding: (a) 50 Ω impedance matching; (b) microstrip line feeding.

4. Antenna fabrication

The patch antennas were fabricated on a flexible polyimide film (Kapton HN) using semiconductor fabrication processes, as illustrated in Figure 3. First, a 50 μm thick Kapton film was cut into 4" × 4" square strips. They were cleaned in ultrasonic acetone bath for a few minutes. Following cleaning, a layer of hexamethyldisiliazane (HMDS) was spin-coated on the Kapton strips at a speed of 2000 rpm for 30 seconds. Positive photoresist S1813 was then spin-coated using the same speed and time, producing a film thickness of 1.5 μm (Figure 3.a). After baking the Kapton strips on a hotplate at 100°C for one minute, the antenna pattern was transferred from a dark field mask to the photoresist by exposing the photoresist with a UV light of 25 mW/cm^2 in intensity for 15 seconds. A photoresist developer MF319 was used to develop

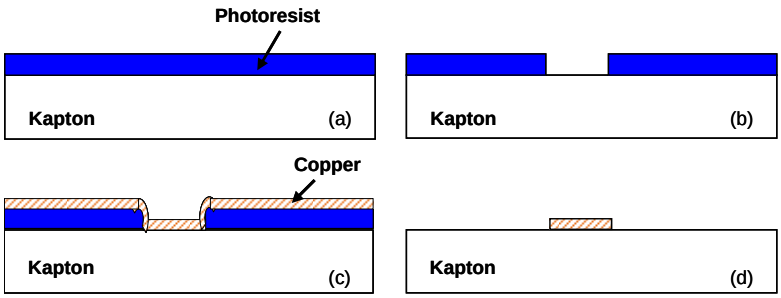

Figure 3: Fabrication steps of the patch antenna.

the antenna patch (Figure 3.b). The developing time was set to be 30 seconds. After developing, the Kapton strips are rinsed with DI water and dried using dry nitrogen air. A copper film of 1 μm in thickness was then deposited on the Kapton strips using thermal evaporation (Figure 3.c). The final fabrication involved soaking the Kapton strips in pure acetone for 3 hours to remove the developed photoresist and lift off the metal on top (Figure 3.d). Since we will bond the antenna to a metallic structure, no ground plane was fabricated on the substrate. The fabricated patch antenna is shown in Figure 4.

5. Mechanical testing of the patch antenna

Mechanical testing of the patch antenna for strain measurement was carried out using a cantilever beam, as shown in Figure 5.a. The antenna sensor was bonded on an aluminum cantilever beam using a conventional strain gauge adhesive. The microwave signal supplied by a network analyzer was fed to the antenna sensor through an SMA connector. The signal reflected by the antenna sensor was routed back to the receiver of the network analyzer, from which the antenna radiation parameters, *i.e.* the S_{11} parameter, can be determined. Weight was added at the free end of the cantilever beam at an increment of 5 lb.

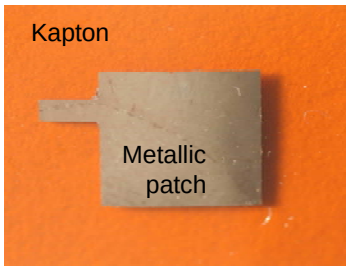

Figure 4: Fabricated patch antenna.

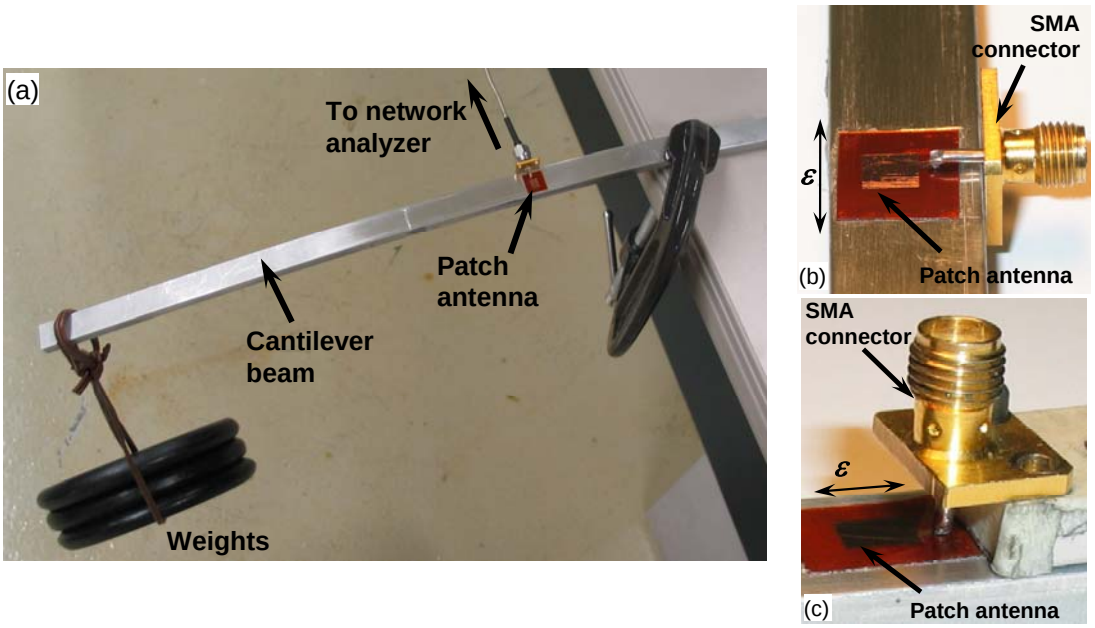

Figure 5: Experimental set up for strain measurement; (a) loading of the cantilever beam; (b) width-direction elongation; (c) length-direction elongation.

In order to stretch the antenna along its width direction, the patch was oriented with its microstrip line perpendicular to the length direction of the cantilever beam (see Figure 5.b). An SMA connector was mounted on the edge of the cantilever with its pin touching the end of the microstrip line. A solder ball was placed at the end of the SMA tip to ensure a sound electrical connection between the SMA tip and the antenna microstrip line. In order to stretch the antenna along its length direction, however, the antenna has to be oriented with its microstrip line parallel to the length direction of the cantilever beam (see Figure 5.c). The only feasible way to feed the patch antenna was then to vertically hold the SMA connector and press the tip of the SMA connector onto the end of the antenna microstrip line.

6. Results and discussions

The design of the dual frequency antenna was verified using a commercial EM simulation tool, Sonnet Pro v11.5. The simulated S_{11} curve of the dual frequency antenna is shown in Figure 6. The two resonant frequencies were found to be f_{10} = 14.9 GHz and f_{01} = 19.6 GHz. The return loss at the f_{01} is higher than that at f_{10} because of better impedance matching for the TM_{01} mode. The S_{11} parameters of the patch antenna under zero loading were measured and compared with the simulated results. The measured patch antenna displayed two resonant frequencies in its S_{11} curve. The length-direction resonant frequency f_{10} was measured at 17.2 GHz while the width-direction resonant frequency f_{01} was measured at 20.5 GHz. The 2 GHz discrepancy between the designed frequency and the measured frequency for the TM_{10} mode was probably

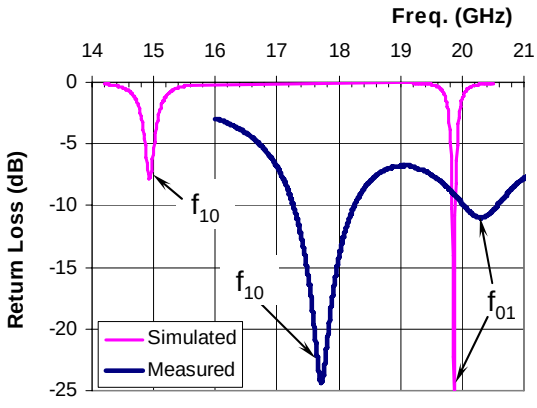

Figure 6: Comparison of simulated and measured antenna S11 curves.

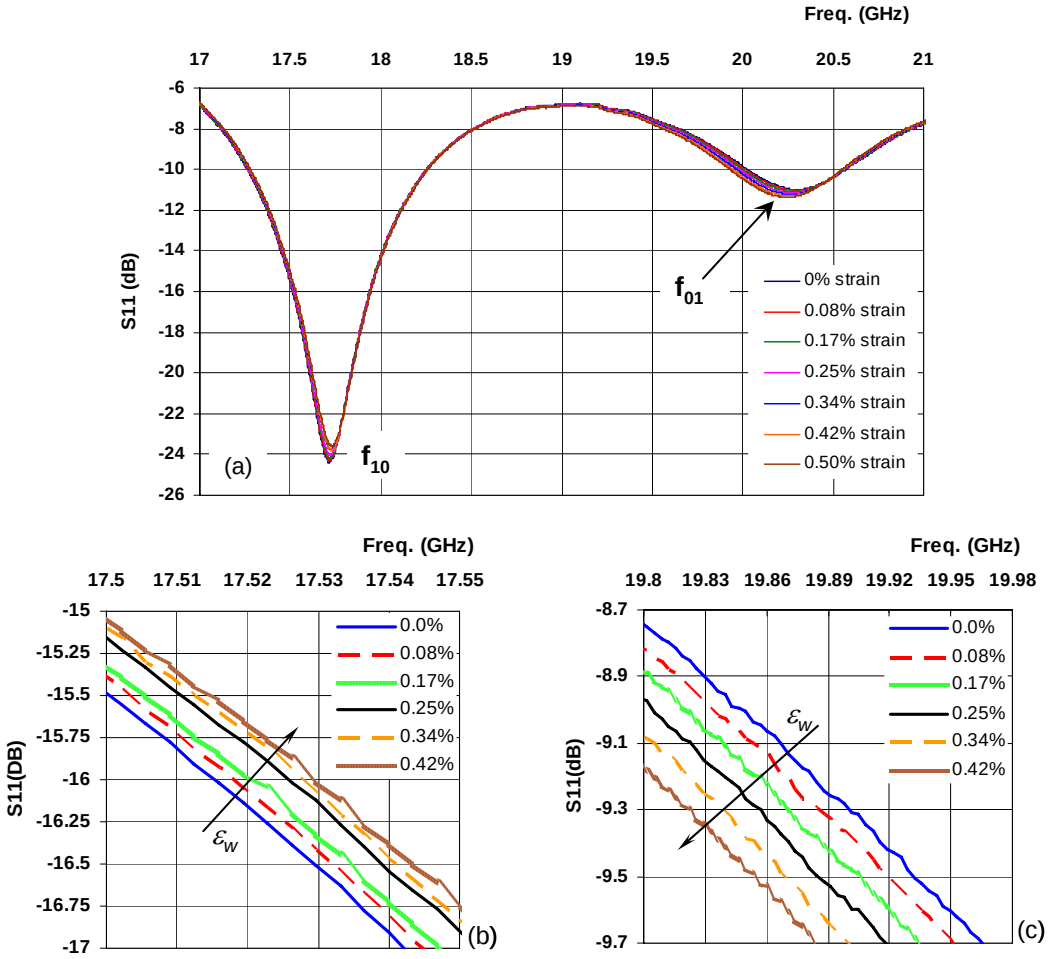

Figure 7: Shifts of S_{11} curves under width-direction strains; (a) overview; (b) shifts of f_{10} frequency-enlarged view; (c) shifts of the f_{01} frequency-enlarged view.

due to the additional capacitance introduced by the SMA connector.

The patch antenna was tested by applying strains along its geometric width direction first. The load was increased at an increment of 5 lb until a total load of 30 lb. At the antenna position, 5 lb of load will lead to 0.084% of strain. The network analyzer was set to acquire 1600 points from 16 GHz to 21.5 GHz. An overview of the measured S_{11} curves under different strain levels is shown in Figure 7.a. Zooming in the regions near the f_{01} and f_{10} frequencies (see Figures 7.b and 7.c) demonstrated the parallel shifts of these two frequencies. The f_{10} frequencies shifted to the right as the strains increased while the f_{01} frequencies shifted to the left. This is consistent with the analytical prediction. The percentages of frequency shifts for these two resonant frequencys, both calculated and measured, were plotted with respect to the applied strains, as shown in Figure 8. Excellent linearity was achieved for both the calculated and measured data. The slopes of the fit lines represent the strain sensitivity of the respective frequency. For the f_{01} frequency, the analytical model predicted a slope of 0.98, which means a 1% strain would shift the f_{01} frequency by 0.98%. The slope of the measured data is 0.81, slightly lower than that of the calculated data. This is probably due to the shear lag introduced by the bonding layer and the Kapton substrate. Expressing the frequency shifts in absolute value, the strain sensitivity of the f_{10} frequency was estimated to be 16.4 kHz/microstrain. Assuming the network analyzer can achieve a 10 Hz

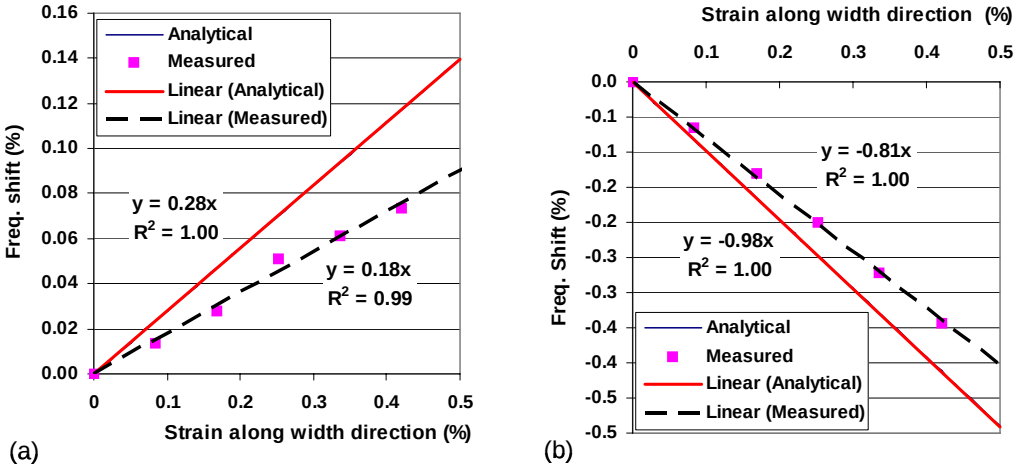

Figure 8: Comparison of analytical and measured strain sensitivities; (a) f_{10} frequency; (b) f_{01} frequency.

frequency resolution, the strain resolution of the antenna sensor is estimated to be 6.1e-4 microstrains. The sensitivity of the f_{01} frequency to the width direction strains is much smaller. With a slope of 0.18, the strain sensitivity in absolute value is 3.3 kHz/microstrain, one fifth of the strain sensitivity of the f_{10} frequency.

When the antenna was strained along its length direction, only the f_{10} frequency can be observed at the network analyzer due to vertical feeding. Therefore, the network analyzer was set to acquire 400 data points from 17.4 GHz to 18.1 GHz. Because the bending of the cantilever beam causes the antenna to slide away from the SMA connector, the antenna had to be mounted close to the fixed end of the cantilever beam. Applying a load of 5 lb at the free end of the cantilever beam will produce a strain of 0.1% at the antenna position. The parallel shifts of the S_{11} curve under various strains are shown in Figure 9.a. Again, we achieved an excellent linearity between the shifts of the f_{10} frequency and the length-direction strains (see Figure 9.b). Moreover, the slope of the measured data matched very well with the theoretical predictions. The sensitivity of the f_{10} frequency with respect to the length-direction strain, around 17.2 kHz/microstrain, is slightly higher than that of the f_{01} frequency when the antenna was under width direction elongation.

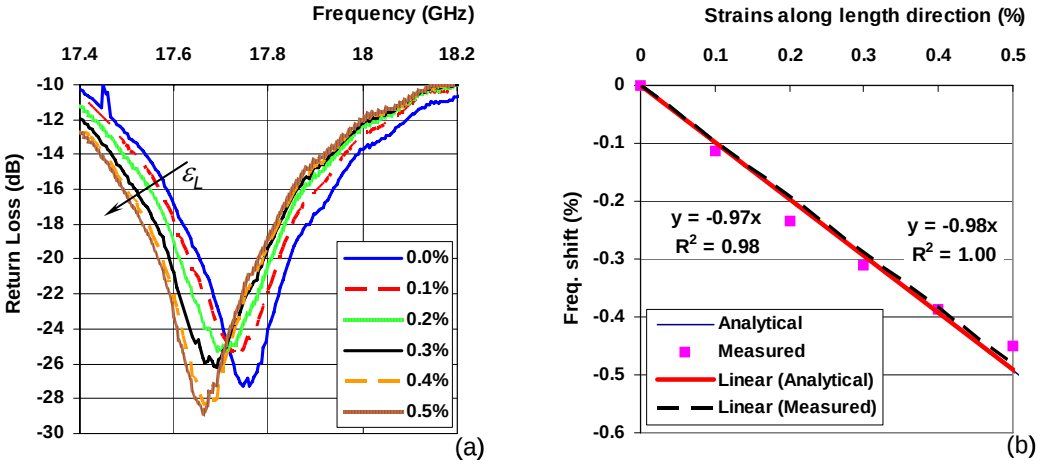

Figure 9: (a) Shifts of f_{10} frequency under length direction strains; (b) comparison of analytical and measured strain sensitivities.

7. Discussion of non-contact measurement of antenna resonant frequency

The antenna resonant frequency can be measured via a non-contact reader, based on the principle of backscattering, as shown in Figure 10. The reader serves as both the transmitter and the receiver. As a transmitter, the reader sends an incident EM wave toward the patch antenna. Upon intercepted by the patch antenna, the incident EM wave is scattered back by the patch antenna if the frequency of the incident wave matches the resonant frequency of the patch antenna. The backscattered EM wave is then received by the reader. By performing frequency analysis of the backscattered EM signals, the antenna radiation parameters (resonant frequency, return loss, *etc.*) can be measured.

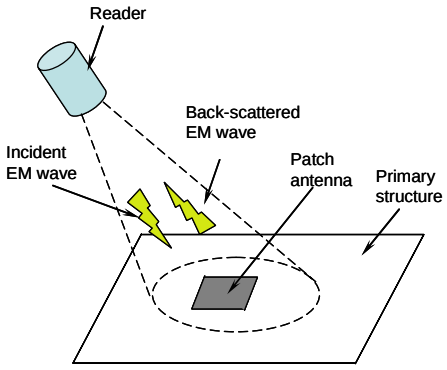

Figure 10: Non-contact interrogation of antenna resonant frequency

Assuming a horn antenna is employed as the antenna reader and it is placed at a distance R from the antenna sensor, the power of the backscattered signal received by the antenna reader can be calculated from the Friis Transmission Equation, i.e.

$$P_r = \frac{P_t G_h^2 G_s^2 \lambda^4 D}{(4\pi R)^4}, \tag{12}$$

where P_t is the transmitting power, G_h is the gain of the horn antennas, G_s is the gain of the antenna sensor, λ is the wavelength, and D is the insertion loss of the sensor. The minimum detectable power at the receiver is calculated as

$$P_{\min} = SNR \times kT \times B \times NF, \tag{13}$$

where SNR is the signal-to-noise ratio, kT is the thermal energy, B is the bandwidth of the receiver, and NF is the noise Figure of the receiver. The maximum distance at which the antenna sensor can be detected is therefore

$$R_{\max} = \frac{\lambda}{4\pi}\left(\frac{DP_t G_h^2 G_s^2}{SNR \times kT \times B \times NF}\right)^{1/4}. \tag{14}$$

For a transmitting power of P_t = 1 mW, G_h = 316 (25 dBi gain), G_s =3.98 (6 dBi gain), λ = 15 mm (RF = 20 GHz), SNR = 100, kT = $4\text{x}10^{-21}$ J, B = 10 kHz, NF = 1, and D = 0.1, the estimated maximum detectable distance is 16.8 meters.

A waveguide was originally used as the antenna reader. As shown in Figure 11, the waveguide is mounted on a three-axis translation stage for proper alignment between its opening and the patch antenna below it. A MATLAB program was developed to time-gate the time domain antenna *S11* signal. By convert the time-

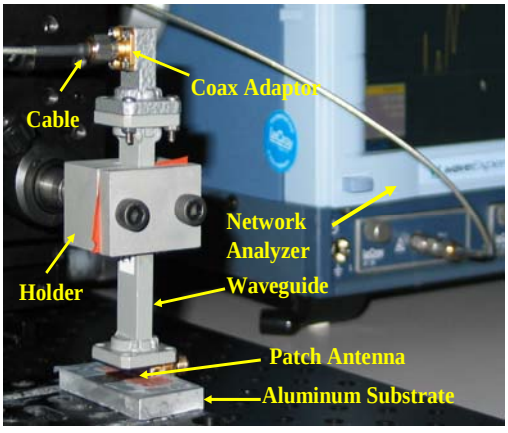

Figure 11: Remote interrogation of antenna resonant frequency using a waveguide

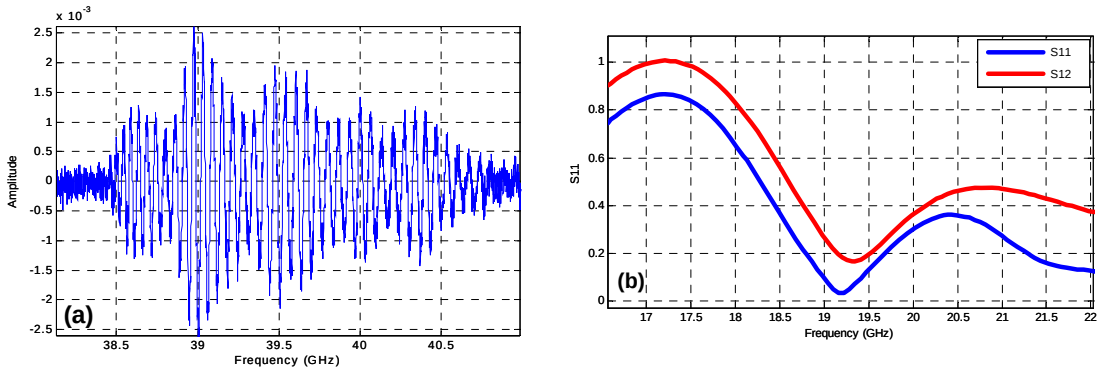

Figure 12: Time gated S11 signal; (1) time-domain; (2) frequency spectrum

gated *S11* signal back into the frequency domain, the antenna resonant frequency can be determined. Figure 12.a shows a typical gated *S11* signal in time domain. The spectrum of the time-gated *S11* signal matched well with the spectrum of the *S12* signal. However, the shifts of the *S11* signal were not consistent with the applied strain when it was tested using the cantilever beam. The challenge facing in using the waveguide as the antenna reader is that the spectrum of the *S11* signal is highly sensitive to the waveguide-antenna alignment. A small movement in the waveguide position will disturb its alignment with the patch. In addition, the waveguide needs to be placed very close to the patch since it has a low directivity. We have also tried to use a horn antenna as the antenna reader. However, the horn antenna usually has a large far-field distance, typically 2.5 meters at 20 GHz. When the antenna is placed at the far-field, the beam size of the horn antenna is very big. Even with time gating, the backscattering of the patch antenna is of low signal strength compared to the strength of background cluttering. Because of the small signal-to-noise ration, it is difficult to determine the frequency of the backscattered signal.

It was decided that a bi-static radar system will help alleviating this problem. As shown in Figure 13, employing two horn antennas, one for transmitting and one for receiving, gives more flexibility in the alignment. By properly align the polarization of the two horn antennas, the background cluttering can be reduced significantly. Due to the long lead time for the second horn antenna, the testing of the bi-static radar system for antenna resonant frequency interrogation will be carried out in the future.

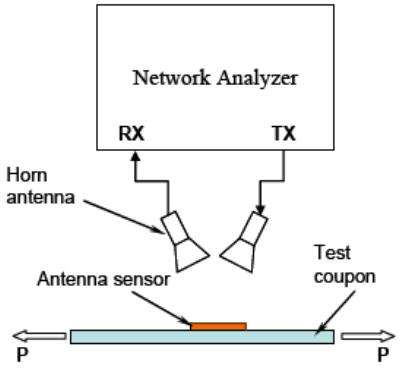

Figure 13: Bi-static radar system for antenna resonant frequency interrogation

8. Conclusions

This report presented the analysis, design, fabrication, and validation of a patch antenna for strain measurement. Both the theoretical analysis and the experiment results demonstrated that the resonant frequency of a patch antenna is sensitive to strains applied along the direction of its corresponding radiation mode. Since the antenna resonant frequency can be remotely interrogated using field coupling or antenna backscattering, the patch antennas have great potentials to serve as passive wireless strain sensor. The development of a wireless radar system that can interrogate the antenna resonant frequency remotely is under way.

Appendix A: List of publications

1. U. Tata, H. Huang, R. Carter, JC Chiao, "Exploiting patch antenna for strain measurement", submitted to *Measurement Science and Technology*
2. U. Tata, H. Huang, R. Carter, JC Chiao, "Passive Wireless Sensor for Strain, Temperature, Crack, and Fatigue Measurement", US provisional patent application
3. U. Tata, "Study of patch antennas for strain measurement", Master thesis, University of Texas at Arlington, Aug. 2008 (available from UTA library)
4. U. Tata, H. Huang, R. Carter, JC Chiao, "Bio-inspired sensor skins for structural health monitoring", to be presented at the ASME Conference on Smart Materials, Adaptive Structures and Intelligent Systems, October 28-30, 2008, Ellicott City, Maryland, USA

Appendix B: Executive summary of Tata's Master thesis

An innovative method of measuring strain using a patch antenna is investigated in this thesis to overcome the limitations of existing wireless strain sensing technologies. The patch antenna is made of a thin sheet of low-loss insulating material, called the dielectric substrate. The antenna pattern, *i.e.* a metallic patch, is printed on one side of the substrate. A ground plane is coated on the opposite side of the dielectric substrate. The metallic patch and the ground plane form an electro-magnetic (EM) cavity. When fed with electromagnetic signal, the patch antenna radiates at a resonant frequency. The antenna resonant frequency depends on its electrical dimensions. Strain changes the dimensions of patch antenna, resulting in a shift in the resonant frequency of patch antenna. First, single frequency and dual frequency antennas are designed using the transmission line model. The antenna design is then confirmed using an Electromagnetic (EM) simulation tool, Sonnet 11.5. Because the dual frequency antenna has two fundamental frequencies f_{010} and f_{010} corresponding to the antenna's geometrical length and width respectively, it is sensitive to strains applied along both directions. The single frequency antenna, however, has only one fundamental frequency f_{010}. Therefore, it is only sensitive to strains applied along the antenna length direction. The effect of strain along the width and length direction of the dual frequency antenna and the width direction of the single frequency antenna on the antenna resonant frequency were simulated using Sonnet 11.5 and the strain sensitivity of the antenna was calculated for each case. The antennas are fabricated on a flexible Kapton substrate using conventional micromachining techniques. The effect of strain on antenna resonant frequency was verified experimentally by bonding the antenna onto a cantilever beam and applying load at one end of the cantilever beam. The experimental and simulated results are in good agreement with each other.

Appendix C: List of software program

1. MATLAB program to simulate the effect of strain on the resonant frequency of a patch antenna based on transmission line model

```
% Calculate the frequency of microstrip patch antenna
% from Bhartia, Rao & Tomar, "Millimeter-wave microstrip and printed
% circuit antennas",Artech House, Boston, 1991, P10-11
% First created: 10/28/2006
clear; clc;

w0=0.004; % width of patch, in meter
L0=0.00533 % length of patch in meter
t0=50e-6; % thickness of substrate, in meter
Epsilon=3.4;  % dielectric constant of the substrate

strain=[0:0.01:1]*1e-2;  % strain of antenna
mu_c=0.3;       % poissons ratio of the conductor
```

```
mu_s=0.3;       % poisson's ratio of the substrate
L=(1+strain)*L0;  % length of patch after strain
w=(1-mu_c*strain)*w0; % width of patch after strain
t=(1-mu_s*strain)*t0; % thickness of the substrate after strain

Rwt=w./t;
%alpha=1+1/49*log((Rwt^4+(1/52*Rwt)^2)/(Rwt^4+0.432))+1/18.7*log(1+(1/18
.1*Rwt).^3);
Ereff=(Epsilon+1)/2+(Epsilon-1)/2*(1+10./Rwt).^(-0.5);  % effective
dielectric constants of substrate
dL=0.412*(Ereff+0.3).*(Rwt+0.264)./(Ereff-0.258)./(Rwt+0.813).*t;  %
line extension

fr=2.998e8/2./sqrt(Ereff)./(L+2*dL);  % resonant frequency of the
antenna

plot(strain*100, fr/1e9); title('Frequency vs. strain');xlabel('strain
(%)');ylabel('R.F (GHz)'); grid on;
(max(fr)-min(fr))/(max(strain)*1e6)
```

2. MATLAB program to evaluate the shift of the S11 curve

```
%interpolation of the frequency values for a given set of returnloss
values
% R is resonant frequency values
% Zero, five, ten, fifteen, twenty,twentyfive and thirty are return
% loss values for all the loads
% xi chosen set of returnloss values
y=[];
zero=load('zero.txt'); % load the return loss values from the txt file
five=load('five.txt');
ten=load('ten.txt');
fifteen=load('fifteen.txt');
twenty=load('twenty.txt');
twentyfive=load('twentyfive.txt');
thirty=load('thirty.txt');
R=load('R.txt');
for xi=-14:-0.1:-15
    Rxi=f_R_xi(thirty, R, xi); % function to interpolated the returnloss
values
    y=[y,Rxi];
end
y(:)

function Rxi=f_R_xi(x, R, xi)
% function Rxi=R_kxi(x, R_meas, xi)
% find the value R at xi if the relationship between x and R is given
% by R at location x. x and R are sort in ascend order
% Inputs:
%   x-sampled locations
%   R-value at sampled locations
%   xi-specified locations
% Outputs:
%   Rxi-value at xi derived from x, R
N=length(xi);
```

```
for ii=1:N
    index=find(x==xi(ii));

    if (length(index)==1)
        Rxi(ii)=R(index);
    else
        index=find(x<xi(ii));
        p_l=index(length(index));
        x_l=x(p_l);
        index=find(x>xi(ii));
        p_h=index(1);
        x_h=x(p_h);
        Rxi(ii)=R(p_l)+(xi(ii)-x_l)/(x_h-x_l)*(R(p_h)-R(p_l));
    end
end

[M,N]=size(R);

if N==1
    Rxi=Rxi.';
end
```

3. MATLAB program for converting the S11 curve to time-domain signal, time gating the time-domain signal, and converting the time-gated signal back to frequency domain

```
function [t, R, fk, Rfft]=f_2port_S(fn)
% this program process the S parameter obtained
% by a two port measurement
% IFFt is used to convert the S parameters to time domain signals
% the data were loaded from fn.mat
%   f: frequency
%   S: S parameter in complex number
% Created on 04/07/08

C=['load ', fn, '.mat'];
eval(C); % load the data

f0=[0:f(2)-f(1):min(f)].';
f=[f0;f];
S12=[zeros(size(f0));S12];
figure; plot(f, abs(S12));title('S parameter'); xlabel('Freq (GHz)');
ylabel('S (dB)'); grid on

Nfft=2^15;

% convert the S data back to time domain
[t, R]=f_ifft_t(S, f(2)-f(1), Nfft);
figure;plot(t, R); title('time domain signal S'); grid on
tl=input('input low cut-off signal: ');
th=input('input high cut-off signal: ');

% window the antenna signal
index=find(t>tl);  % cut-off the signals at the begining
tc=t(index);
Rc=R(index);
index=find(tc<th); % high cut-off
tc=tc(index);
```

```
Rc=Rc(index);
%Rc=Rc.*hanning(length(Rc));

Ntc=length(tc);

[fk, Rfft]=f_fft_fk(Rc, 1/(tc(2)-tc(1)), Nfft);

figure; plot(tc, Rc);title('Windowed time domain signal'); xlabel('time
(ns)'); ylabel('Amp'); grid on;
figure;  plot(fk, Rfft/max(Rfft)); title('S from windowed time domain
signal'); grid on;axis([0 50 0 1]);
xlabel('Freq (GHz)'); ylabel('amp');

return;

function [t, Rifft]=f_ifft_t(Rcfft, fs, Nfft)
% this function convert a frequency domain signal to time domain signal
% Inputs:
%   Rcfft: frequency domain signal in complex
%   fs: frequency sampling rate
%   Nfft: number of inverse FFT
% Outputs:
%   t: time
%   Rifft: signal in time domain, obtained from inverse fft

Rifft=ifft(Rcfft, Nfft);  % digital inverse fft
Rifft=real(Rifft(1:floor(Nfft/2))); % the real part only
t=1/fs*[0:floor(Nfft/2)-1]/Nfft;

return

function [fk, Rfft]=f_fft_fk(R, fs, Nfft)
% function [fk, Rfft]=fft_fk(R, fs, Nfft)
% find the FFT of R as a function of frequency fk
% Inputs:
%    R: signal
%    fs: sampling frequency
%    Nfft: # of fft
% Outputs:
%    fk: frequency
%    Rfft: real value of fft(R)

Rfft=abs(fft(R, Nfft));  % fft of signal R
Rfft=Rfft(1:floor(Nfft/2));
fk=fs*[0:floor(Nfft/2)-1]/Nfft;
return
```